probability (P) = 0.03.
19. Data were gathered for 28 moths puddling on three Na solutions: 0.01 mM (n = 8), 0.1 mM (n = 10), and 1 mM (n = 10). The slope ± 1 SE of linear regression (Na uptake versus K loss, expressed as micromoles per moth) was 0.97 ± 0.15, coefficient of determination (r^2) = 0.62, $P < 0.001$.
20. Males were paired to minimize differences in age and relatedness. Within a pair, one moth was randomly assigned to puddle (solution as in Fig. 2B), and the other was kept without fluid as a control (if former moth failed to puddle, the pair was discarded). After puddling (16 ± 1 hours after cessation), pair members were dissected (in the dry) into four components: reproductive system (testes, simplex, accessory glands); gut (complete digestive system, including malpighian tubules); coremata (the pheromonal brushes) plus genitalia; and remains (all other parts combined). Dissected parts were oven-dried (55°C) and weighed, then digested [quartz tubes; boiling mixture of 0.25 ml of nitric acid (70%) and 0.10 ml of perchloric acid (70%)], taken to dryness, solubilized [0.15 ml of hydrochloric acid (37%)], and brought to 3.00 ml with quartz-distilled water, then analyzed (*14*).
21. The puddling solution was as in Fig. 2B, and the analytical technique was as in (*14, 20*) except that the digestion step (*20*) was done twice.
22. The energetic cost of fluid transport through a tube decreases linearly with shortening and exponentially (fourth power) with bore increase [M. LaBarbera and S. Vogel, *Am. Sci.* **70**, 54 (1982)].
23. J. S. Miller, *Bull. Am. Mus. Nat. Hist.* **204**, 1 (1991).
24. S. R. Smedley, thesis, Cornell University, Ithaca, NY (1993).
25. Ileal length and midpoint width were as follows: males (13.9 ± 1.8 mm and 0.30 ± 0.06 mm; n = 11); females (8.4 ± 1.3 mm and 0.15 ± 0.02 mm; n = 10). Independent t tests for both between-sex comparisons: $P < 0.001$.
26. The surface area of the ileal lining was estimated from the gross linear measurements (*25*) and from measurements from electronmicrographs (Fig. 1D), which provided a basis for calculation of villi dimension and numbers (the villus was assumed to be a right circular cone).
27. W. R. Harvey, in *Insect Biology in the Future*, M. Locke and D. S. Smith, Eds. (Academic Press, New York, 1980), pp. 105–124; J. E. Phillips, J. Hanrahan, M. Chamberlin, B. Thomson, *Adv. Insect Physiol.* **19**, 329 (1986).
28. Leaf samples were taken fresh from aspen (Ithaca, NY). After they were oven dried (55°C) and ground, the samples (0.4 g each) were dry ashed (450°C, 6 hours) in quartz tubes. On cooling, 0.25 ml of hydrogen peroxide (30%) was added, and samples were ashed (2 hours). The ash was then solubilized as in (*20*), except that 0.5 ml of hydrochloric acid and 9.5 ml of water were added. Analyses as in (*14*).
29. G. E. Likens and F. H. Bormann, *Chemical Analyses of Plant Tissues from the Hubbard Brook Ecosystem in New Hampshire* (Yale School of Forestry Bulletin 79, Yale University, New Haven, CT, 1970); D. B. Botkin, P. A. Jordan, A. S. Dominski, H. S. Lowendorf, G. E. Hutchinson, *Proc. Natl. Acad. Sci. U.S.A.* **70**, 2745 (1973); D. H. Pletscher, thesis, Yale University, New Haven, CT (1982).
30. Calculation based on (*1*).
31. For both measures [variances showed heteroscedasticity (Bartlett's test; $P < 0.001$) that remained after logarithmic transformation], significant differences were detected between treatments [Kruskal-Wallis analysis of variance: duration, H = 23.1, degrees of freedom (df) = 2, $P < 0.001$; volume, H = 22.7, df = 2, $P < 0.001$].
32. We thank D. Deutschman, M. Eisner, P. Fraissinet, J. Franclemont (to whom this paper is fondly dedicated), J. F. Hare, H. Hurrell, K. Moy, M. Oliva, M. Rutzke, and M. VanEvery for assistance. Supported by NIH grant AI 02908 and a National Institute of Mental Health training grant, the Edna Baily Sussman Fund, Sigma Xi, the Theodore Roosevelt Memorial Fund, and Cornell Graduate School stipends.

16 June 1995; accepted 14 September 1995

Evidence for Developmentally Programmed Transdifferentiation in Mouse Esophageal Muscle

Ardem Patapoutian,* Barbara J. Wold,† Roger A. Wagner‡

Transdifferentiation is a relatively rare phenomenon in which cells of one differentiated type and function switch to a second discrete identity. In vertebrate embryos, smooth muscle and skeletal muscle are distinct tissues that arise from separate compartments of the mesoderm. The musculature of the mouse esophagus was found to undergo a conversion from smooth muscle in the fetus to skeletal muscle during early postnatal development. The switch from smooth to skeletal muscle features the transitory appearance of individual cells expressing a mixed phenotype, which suggests that this conversion is a result of programmed transdifferentiation.

Skeletal and smooth muscles of vertebrates differ with respect to structure, innervation, function, and developmental origin (*1*). For example, skeletal muscle is composed of fused multinucleate myotubes containing striated fibers, whereas smooth muscle is composed entirely of mononucleate, nonstriated cells. The musculature of the mammalian stomach and intestine is composed exclusively of smooth muscle, but the esophagus differs because it also contains skeletal muscle. Although some muscle genes are expressed in both smooth and skeletal muscle tissues, others are strictly specific.

Division of Biology, California Institute of Technology, Pasadena, CA 91125, USA.

*Present address: Howard Hughes Medical Institute, University of California, San Francisco, CA 94143, USA.
†To whom correspondence should be addressed.
‡Present address: Department of Internal Medicine, University of Colorado School of Medicine, Denver, CO 50262, USA.

By monitoring the expression of such highly specific smooth or skeletal muscle markers [skeletal fast myosin heavy chain (MHC) and smooth myosin light chain (MLCK)], we found that during early development, the mouse esophageal musculature is composed entirely of differentiated smooth muscle (Fig. 1, A and B) (*2, 3*). Later, esophageal expression of smooth muscle–specific genes declines and expression of skeletal muscle–specific genes increases (Fig. 1, C through F). This transition from smooth to skeletal muscle type occurs in a rostrocaudal progression that begins in late fetal development and continues through the first 2 weeks of postnatal development (Fig. 1, G and H). Smooth muscle myosin heavy chain, another smooth muscle–specific marker, was also expressed in the esophageal musculature at prenatal time points, which confirmed the smooth muscle phenotype of these cells (*3, 4*). The expression pattern of another skeletal muscle–specific protein, α-actinin, was the same as that of skeletal MHC protein for all developmental time points (*5*).

The muscularis layer of diaphragm-level esophagus expressed both skeletal and smooth muscle proteins at postnatal day 3 (P3), which revealed a time and place of transition at the tissue level (Fig. 1C). Greater magnification revealed coexpression of smooth MLCK and skeletal MHC in the cytoplasm of individual cells (Fig. 1D). This unanticipated coexpression of smooth and skeletal differentiation markers within individual cells was observed from embryonic day 16 (E16) in rostral sections to P8 in caudal sections (*5*). Coexpression on the single-cell level was verified by partial dissociation of P3 esophagus tissue (Fig. 1, I through L). The progression from smooth to skeletal tissue type, together with the coexpression of smooth and skeletal markers in individual cells, suggests that functional, differentiated smooth muscle cells in the esophagus switch directly to differentiated skeletal myocytes. The presence of syncytial myofibers in dissociated preparations provided additional cytological evidence for the skeletal character of the final muscle phenotype (*5*).

Expression of the skeletal muscle regulatory factors (MRFs) MyoD, myogenin, Myf-5, and MRF4 marks commitment to the skeletal muscle phenotype, but extensive studies of their expression patterns have never found these markers in smooth muscle or its known progenitors. At least one of the MRFs is expressed before transcription of any muscle-specific structural gene in all skeletal muscle (*6*). At E15 (Fig. 2, A and B) and at birth (*5*), diaphragm-level esophageal musculature was consistent with this pattern and did not stain with monoclonal antibodies (mAbs) to MyoD or myogenin,

whereas smooth muscle–specific MLCK was highly expressed. In situ hybridization studies also showed that Myf-5 and MRF4 RNAs were not expressed in the muscularis layer of diaphragm-level esophagus at E15 (5). Shortly after birth, the diaphragm-level esophageal musculature expressed myogenin (Fig. 2C) and MyoD (5) as well as MLCK. Myogenin was localized within the nucleus of cells that expressed cytoplasmic smooth muscle MLCK (Fig. 2D), and this observation was verified by examination of dissociated esophagus tissue (5). We conclude that the expression of smooth muscle differentiation genes precedes the expression of all four MRFs, and this supports the idea that the esophagus muscularis begins as differentiated smooth muscle before it commits to a skeletal muscle phenotype.

The mixed cell phenotype suggests that the tissue-level conversion from smooth to skeletal muscle occurs by direct transdifferentiation at the cellular level. However, only a small percentage of cells were seen to express this mixed phenotype at any given time. Although this finding would be expected if the transdifferentiation were quite rapid, there is an alternative (albeit more complex) model: Cells expressing mixed phenotypes may be fated to die, and the main body of skeletal muscle may come from a population of precursor cells that had never assumed a smooth muscle phenotype. To discriminate between these possibilities, we first attempted to physically mark individual smooth muscle cells of the early esophagus to trace their fate at later times, but we were unable to do so because the esophagus proved inaccessible for surgical manipulation. We then assayed apoptosis by terminal deoxynucleotidyl transferase–mediated deoxyuridine triphosphate nick end-labeling (TUNEL) and propidium iodide staining at various rostrocaudal levels and developmental time points. No muscle cell death in the muscularis layer was detected, in contrast with the results for thymus controls (Fig. 3, A through D) (5). When E18 and P5 mice were labeled with 5-bromo-2′-deoxyuridine (BrdU), only a moderate level of cell proliferation was seen in the muscularis layer, and many of the dividing cells were in the smooth muscle population (Fig. 3, E and F) (5); these findings argue against the presence of a major population of dividing (nonsmooth muscle) skeletal muscle precursor cells. Thus, a mechanism that features simultaneous smooth muscle cell death and skeletal muscle replacement remains an interesting possibility, but we did not find direct evidence to support it. Moreover, this model fails to provide an explanation for the emergence of mixed phenotype cells. In the alternate model, direct transdifferentiation is the principal mechanism for the smooth skeletal transition; we currently favor this model because it is consistent with all of the data, provides a clear function for the mixed phenotype cells, and is appealing in its simplicity.

Transdifferentiation is thought to be a relatively rare phenomenon (7). Prominent examples such as amphibian limb regeneration and chick retina regeneration occur in response to injury (8), whereas the conversion of neural crest–derived adrenal chromaffin cells into sympathetic neurons occurs under experimental manipulations (9). In contrast, the esophageal smooth muscle–skeletal muscle conversion is part of the normal developmental program, and it is therefore most similar to the perinatal switch in the neurotransmitter phenotype of sympathetic neurons that innervate sweat glands (10).

A major theme in vertebrate development is that sequential changes in the repertoire of expressed genes lead progenitor cells to their mature, differentiated state by means of a series of changes in cellular phenotype. Well-known instances of transdifferentiation often involve dedifferentiation followed by execution of an alternate differentiation pathway (7). The apparent "jump" from the end product of one pathway directly to the end product of a different pathway is, therefore, a surprising phenomenon and immediately raises questions about the underlying mechanism. The regulatory properties of MyoD family skeletal

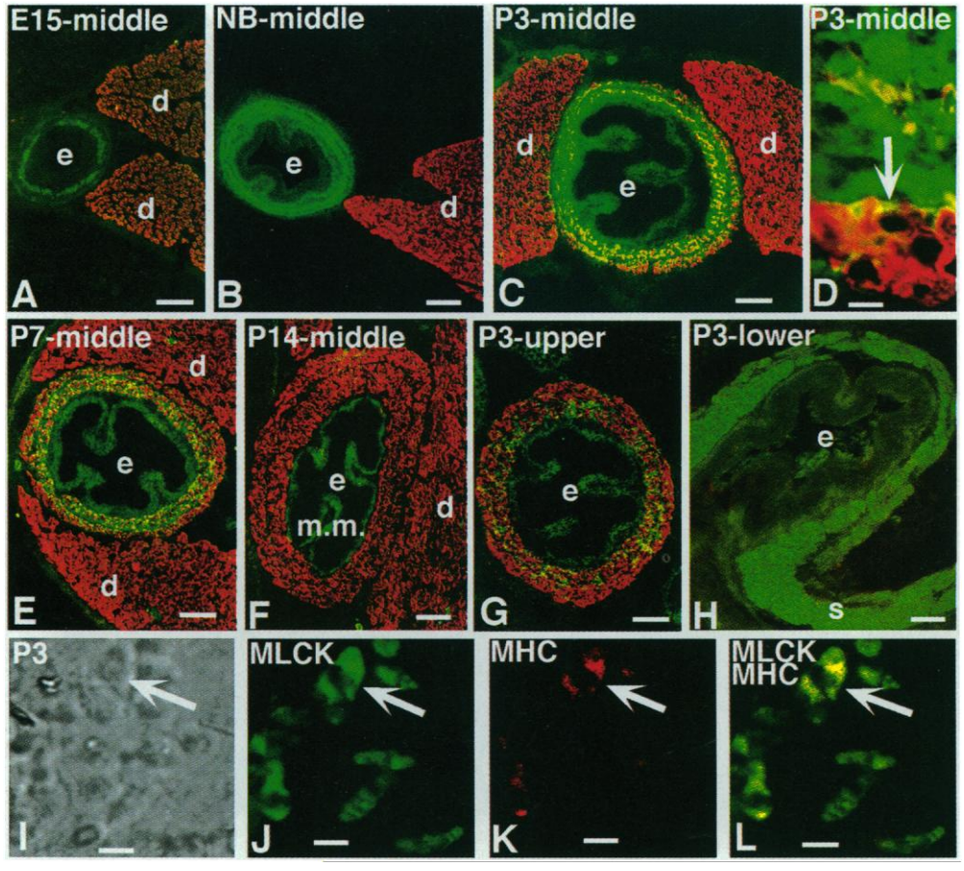

Fig. 1. Developmental rostrocaudal transition from smooth to skeletal muscle in the muscularis layer of the mouse esophagus, as shown by confocal microscope images. Esophageal tissue transverse sections and dissociated cells were labeled with MLCK mAb (green) and fast MHC mAb (red) (*13*); colocalization of MLCK and MHC appears as yellow. (**A** through **F**) Developmental series of diaphragm-level (middle) sections at the indicated embryonic and postnatal days (NB, newborn). In (D), a magnification of (C), the arrow points to a cell coexpressing both markers. (**G** and **H**) Upper and lower esophagus sections of P3 mice; comparison with (C) shows the rostrocaudal gradient. The muscularis mucosae (the inner thin layer of muscle in the esophagus) expresses only smooth muscle–specific MLCK at all times, and the nearby diaphragm exclusively expresses skeletal muscle–specific MHC. (**I** through **L**) Phase image (I) and fluorescent images (J through L) of a group of P3 dissociated esophageal cells; arrows point to cells that express both markers. Dissociation experiments were carried out by gentle mechanical disruption of tissue followed by collagenase and dispase treatment for 15 min at 37°C (*14*). Abbreviations: d, diaphragm; e, esophagus; m.m., muscularis mucosae; s, stomach. Scale bars, 5 μm (D and I through L); 100 μm, all other panels.

muscle regulatory factors (MRFs) suggest a candidate mechanism. Experimentally induced ectopic expression of the MRFs can dominantly convert various terminally differentiated cells (including primary smooth muscle cells in culture) to a skeletal muscle phenotype (*11*). In the esophageal muscle pathway, evolution may have capitalized on the potential of MRFs to drive a direct transition to skeletal muscle. Because smooth and skeletal muscle share a general contractile function, a direct shift from one to the other that preserves function during the transition might be an attractive option, especially because this transition occurs mainly after birth, when feeding requires esophageal peristalsis. In support of this idea, there is a second candidate case for a muscle conversion in the avian eye, where there is evidence that during embryonic development this muscle expresses smooth muscle–specific genes as a transition state to mature skeletal muscle (*12*). No information is yet available on MRF expression in the chick iris muscle, but if the process is similar to that seen in the esophagus, MRF involvement would be expected.

This initial characterization of a smooth muscle–skeletal muscle transition and its relation to current knowledge about the molecular and developmental determinants of myogenesis leaves many questions unanswered. Although activation of MyoD family regulators may drive the transition, it is unclear what triggers them to be expressed or which events lead to the down-regulation of smooth muscle genes. Similarly, the origin and nature of the inductive interactions that regulate the slow rostrocaudal wave of skeletal differentiation are unknown. Finally, the origin of muscle cells in the esophagus has previously received little attention, but in light of our findings, lineage studies to probe the contribution to the esophagus from possible progenitors including somitic and lateral mesoderm should be of interest.

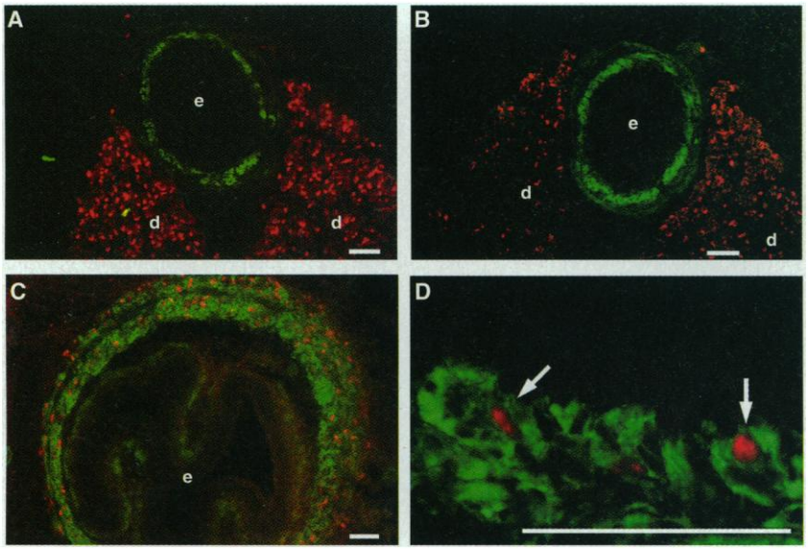

Fig. 2. Expression of smooth muscle–specific differentiation genes precedes expression of the MRFs during esophageal development. Transverse sections through diaphragm-level esophagus of E15 embryos (**A** and **B**) and P3 mice (**C** and **D**) were labeled with MLCK mAb (green) and either myogenin mAb (A, C, and D) or MyoD mAb (B) (red). In (D), a magnification of (C), arrows denote cells that coexpress nuclear myogenin and cytoplasmic MLCK. Abbreviations: d, diaphragm; e, esophagus. Scale bars, 50 μm.

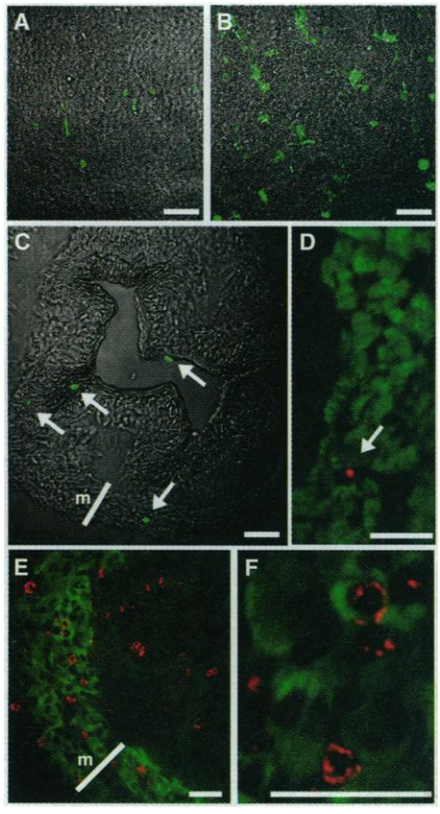

Fig. 3. Cell death and proliferation during perinatal development of the mouse esophagus. Apoptosis was monitored by TUNEL and propidium iodide staining. (**A** through **C**) Superimposed confocal images of phase and TUNEL (FITC, green) staining on 7-μm transverse sections of paraffin-embedded tissues. Thymus tissue from 4-week-old mice was used as a positive control (ApopTag Fluorescein Kit S7110; Oncor). Thymus from untreated mice showed a moderate density of apoptotic cells (A), whereas thymus from mice treated with 50 μg of cortisone acetate (NDC 006-7069-10; Merck) for 12 hours showed the expected large number of clustered pyknotic nuclei (B) (*15*). In (C), TUNEL labeling of diaphragm-level P3 mouse esophagus shows four positive nuclei (arrows), and only one of them is in the muscularis layer (m). (**D**) Frozen section of a diaphragm-level P3 esophagus colabeled with propidium iodide (red) and MLCK mAb (green). The pyknotic cell (arrow) in the muscularis layer does not express MLCK and thus is not a muscle cell undergoing phenotypic transition. Propidium iodide staining was done as described (*16*); tissues were fixed in 4% paraformaldehyde, sectioned, stained for muscle-specific antibodies, and then incubated with 4 μg of propidium iodide (Sigma) and RNase (100 μg/ml, DNase free; Sigma) in phosphate-buffered saline for 30 min at 37°C. (**E** and **F**) Upper esophagus sections from E18 embryos in vivo labeled with BrdU were colabeled with BrdU mAb (red) and MLCK mAb (green); (F) is a magnification of (E). BrdU labeling was achieved by injecting a female at E18 gestation with 20 μl of 10 mM BrdU (1299964; Boehringer Mannheim) per gram of body weight for 4 hours. Scale bars, 25 μm.

REFERENCES AND NOTES

1. C. L. Prosser, *Comparative Animal Physiology* (Saunders, Philadelphia, ed. 3, 1973), pp. 719–788.
2. J.-L. Dubond, *et al.*, *Differentiation* **55**, 1 (1993).
3. A. Patapoutian *et al.*, unpublished results.
4. J. M. Miano *et al.*, *Circ. Res.* **75**, 803 (1994).
5. A. Patapoutian *et al.*, data not shown.
6. M. Buckingham, *Trends Genet.* **8**, 144 (1992).
7. T. S. Okada, *Transdifferentiation: Flexibility in Cell Differentiation* (Clarendon, Oxford, 1991).
8. P. F. Hitchcock and P. A. Raymond, *Trends Neurosci.* **15**, 103 (1992); J. P. Brockes, *Trends Genet.* **10**, 169 (1994).
9. P. H. Patterson, *Cell* **62**, 1035 (1990); D. J. Anderson, *Trends Genet.* **5**, 175 (1989).
10. S. C. Landis, *Trends Neurosci.* **8**, 344 (1990).
11. H. Weintraub *et al.*, *Proc. Natl. Acad. Sci. U.S.A.* **86**, 5434 (1989); J. Choi *et al.*, *ibid.* **87**, 7988 (1990); J. H. Miner *et al.*, *Development* **114**, 853 (1992); H. M. Blau, *Annu. Rev. Biochem.* **61**, 1213 (1992).
12. P. Volpe *et al.*, *Dev. Biol.* **159**, 441 (1993).
13. Transverse frozen sections of embryos (7 to 20 μm), or dissociated esophageal cells attached to polylysine-treated slides, were fixed in 4% paraformaldehyde and blocked for 10 to 20 min in 10% goat serum and 3% bovine serum albumin (BSA) in phosphate-buffered saline before applying the primary antibody in 3% BSA in phosphate-buffered saline for 1 to 3 hours at room temperature. The secondary antibody solution was applied for 1 hour. Antibodies used were myogenin mAb F5D [1:5 dilution; mouse immunoglobulin G1 (IgG1)], MyoD mAb NCL-MyoD1 (1:10 dilution; mouse IgG1; Novocastra Lab.), fast MHC mAb M-4276 (1:400 dilution; mouse IgG1; Sigma), α-actinin mAb A-7811 (1:400 dilution; mouse IgG2b; Sigma), MLCK mAb M-7905 (1:1000 dilution; mouse IgG2b; Sigma), and BrdU mAb MAS

250 (1:10 dilution; rat IgG2a; Sera-Lab). Secondary antibodies to mouse IgG1 and IgG2b or rat IgG were conjugated to fluorescein isothiocyanate (FITC) or tetramethyl rhodamine isothiocyanate and used at 1:100 dilution in 3% BSA in phosphate-buffered saline (Southern Biotechnology Associates). When BrdU mAb was used, the sections were treated for 15 min in 4 M HCl before the blocking step. Images were captured digitally on a BioRad confocal microscope.
14. T. A. Rando and H. M. Blau, *J. Cell Biol.* **125**, 1275 (1994). A nylon mesh was not used.
15. C. D. Surh and J. Sprent, *Nature* **372**, 100 (1994).
16. H. S. R. Coles *et al.*, *Development* **118**, 777 (1993).
17. We thank X. Yu for her work on apoptosis, S. Fraser and K. Woo for imaging and lineage tracing assistance, W. Wright for myogenin mAb cell line F5D, N. Shah for antibodies, J. Miano and E. Olson for SM-MHC plasmid, C. Cardell for technical assistance, and D. Anderson, P. Garrity, N. Hong, J. Miner, P. Mueller, P. Patterson, and members of Wold group for comments. Supported by NIH grant AR40708 to B.W. A.P. was supported by an NIH Predoctoral Training Grant.

10 July 1995; accepted 6 November 1995

Crystal Structure of the V_α Domain of a T Cell Antigen Receptor

Barry A. Fields, Bertram Ober, Emilio L. Malchiodi, Marina I. Lebedeva, Bradford C. Braden, Xavier Ysern, Jin-Kyoo Kim, Xuguang Shao, E. Sally Ward, Roy A. Mariuzza*

The crystal structure of the V_α domain of a T cell antigen receptor (TCR) was determined at a resolution of 2.2 angstroms. This structure represents an immunoglobulin topology set different from those previously described. A switch in a polypeptide strand from one β sheet to the other enables a pair of V_α homodimers to pack together to form a tetramer, such that the homodimers are parallel to each other and all hypervariable loops face in one direction. On the basis of the observed mode of V_α association, a model of an $(\alpha\beta)_2$ TCR tetramer can be positioned relative to the major histocompatibility complex class II $(\alpha\beta)_2$ tetramer with the third hypervariable loop of V_α over the amino-terminal portion of the antigenic peptide and the corresponding loop of V_β over its carboxyl-terminal residues. TCR dimerization that is mediated by the α chain may contribute to the coupling of antigen recognition to signal transduction during T cell activation.

T lymphocytes recognize a wide variety of antigens through highly diverse cell-surface glycoproteins known as TCRs. These molecules are composed of α and β (or γ and δ) chains that have variable (V) and constant (C) regions homologous to those of antibodies (*1*). However, antibodies recognize antigen in intact form, whereas TCRs recognize antigen only as peptide fragments bound to molecules of the major histocompatibility complex (MHC) (*2*). The three-dimensional structure of the extracellular portion of the β chain of a murine TCR (V_α4.1-J_α2B4, V_β8.2-J_β2.1) specific for a hemagglutinin peptide of influenza virus (HA-110–120) in the context of the MHC class II I-E^d molecule has been solved (*3*). A TCR designated 1934.4, which is specific for the NH_2-terminal nonapeptide of myelin basic protein (Ac1–9) in association with I-A^u (*4*), is encoded by the closely related V_α4.2-J_α4.0, V_β8.2-J_β2.3 gene combination (*5*). Injection into mice of the T cell clone from which the 1934.4 TCR was isolated induces experimental autoimmune encephalomyelitis, a model for human multiple sclerosis (*6*). The V_α domain of this pathogenic TCR has been produced and crystallized (*7*, *8*); here, we describe its crystal structure at 2.2 Å resolution (*9*).

The V_α domain exists as a homodimer both in solution (*8*) and in the crystal structure (Fig. 1A). The relative orientation of the two chains in the homodimer is almost identical to that in antibody V_LV_H dimers, with peptide loops homologous to the complementarity-determining regions (CDRs) of antibodies disposed to form part of the antigen-binding site. Fourteen residues from each V_α domain contribute numerous van der Waals contacts and 10 hydrogen bonds across the homodimer interface. Of these, residues Tyr^{35}, Gln^{37}, Pro^{43}, Tyr^{87}, and Phe^{106} [numbered as in (*10*)] are equivalent by homology to those involved in V_LV_H association (*11*, *12*). These residues are also highly conserved in V_β regions (excluding Pro^{43}, which is most commonly substituted by Leu), which indicates that the geometry of TCR

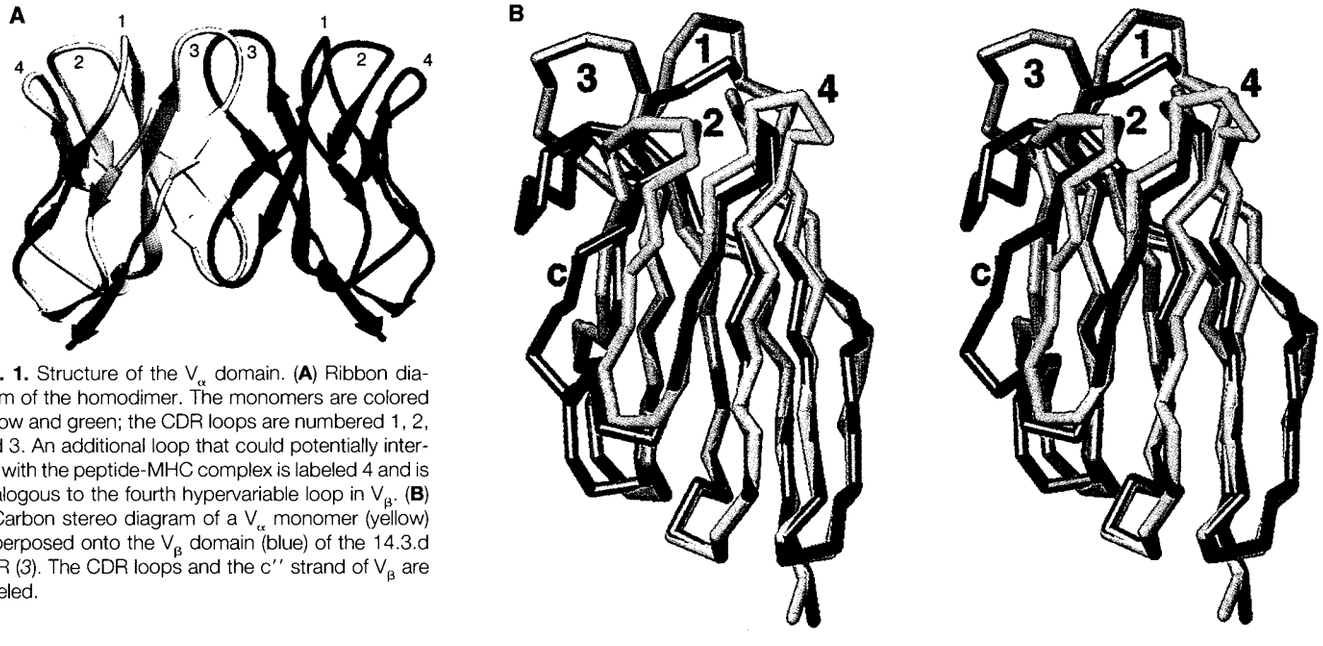

Fig. 1. Structure of the V_α domain. (**A**) Ribbon diagram of the homodimer. The monomers are colored yellow and green; the CDR loops are numbered 1, 2, and 3. An additional loop that could potentially interact with the peptide-MHC complex is labeled 4 and is analogous to the fourth hypervariable loop in V_β. (**B**) α-Carbon stereo diagram of a V_α monomer (yellow) superposed onto the V_β domain (blue) of the 14.3.d TCR (*3*). The CDR loops and the c′′ strand of V_β are labeled.